J Neurophysiol 92: 2933–2946, 2004.
First published June 30, 2004; 10.1152/jn.00450.2004.

Functional Topography of Converging Visual and Auditory Inputs to Neurons in the Rat Superior Colliculus

Irini Skaliora, Timothy P. Doubell, Nicholas P. Holmes, Fernando R. Nodal, and Andrew J. King
University Laboratory of Physiology, University of Oxford, Oxford OX1 3PT, United Kingdom

Submitted 30 April 2004; accepted in final form 21 June 2004

Skaliora, Irini, Timothy P. Doubell, Nicholas P. Holmes, Fernando R. Nodal, and Andrew J. King. Functional topography of converging visual and auditory inputs to neurons in the rat superior colliculus. *J Neurophysiol* 92: 2933–2946, 2004. First published June 30, 2004; 10.1152/jn.00450.2004. We have used a slice preparation of the infant rat midbrain to examine converging inputs onto neurons in the deeper multisensory layers of the superior colliculus (dSC). Electrical stimulation of the superficial visual layers (sSC) and of the auditory nucleus of the brachium of the inferior colliculus (nBIC) evoked robust monosynaptic responses in dSC cells. Furthermore, the inputs from the sSC were found to be topographically organized as early as the second postnatal week and thus before opening of the eyes and ear canals. This precocious topography was found to be sculpted by $GABA_A$-mediated inhibition of a more widespread set of connections. Tracer injections in the nBIC, both in coronal slices as well as in hemisected brains, confirmed a robust projection originating in the nBIC with distinct terminals in the proximity of the cell bodies of dSC neurons. Combined stimulation of the sSC and nBIC sites revealed that the presumptive visual and auditory inputs are summed linearly. Finally, whereas either input on its own could manifest a significant degree of paired-pulse facilitation, temporally offset stimulation of the two sites revealed no synaptic interactions, indicating again that the two inputs function independently. Taken together, these data provide the first detailed intracellular analysis of convergent sensory inputs onto dSC neurons and form the basis for further exploration of multisensory integration and developmental plasticity.

INTRODUCTION

The superior colliculus (SC) plays a critical role in the control of orienting movements of the head and eyes toward external stimuli, irrespective of their modality (Stein and Meredith 1993). To do this, spatial information from different sensory modalities has to be combined and represented in the SC in the same coordinates. Many neurons in the deeper layers of the SC (dSC) are multisensory, in that they respond to combinations of visual, auditory, and/or somatosensory stimuli. Furthermore, the receptive fields of these cells are arranged to form topographically aligned spatial maps (King and Palmer 1983; Stein et al. 1975). For the visual modality, the map reflects the spatial order already present in the retina, which is then relayed to the superficial layers of the SC (sSC) and other brain structures. For the auditory modality, however, the receptor surface in the cochlea is organized tonotopically. Therefore, a topographic representation of auditory space has to be computed within the central auditory pathway and aligned in the SC with the coordinates of visual space (King 1999). The construction of overlapping sensory representations facilitates the multisensory enhancement of dSC responses to stimuli that are likely to be derived from the same event. This is thought to underlie improvements in the localization of such stimuli (Burnett et al. 2004; Stein and Meredith 1990).

Previous studies have indicated that signals from the visual system are used to guide the formation of the topographic representation of auditory space (King 1999). Degradation of visual inputs by binocular eyelid suture in young ferrets (King and Carlile 1993) and owls (Knudsen et al. 1991) caused abnormalities in the organization of the auditory space map in the SC. In guinea pigs, dark rearing, which completely eliminates all visual information, was found to result in dSC cells with broad auditory spatial receptive fields and an auditory representation that showed little or no topographic order (Withington et al. 1994). Other studies have investigated more directly the effect of an experimentally induced misalignment of the auditory and visual maps in the SC. Raising owls with prismatic spectacles (Knudsen and Brainard 1991) or removing one of the extraocular muscles in young ferrets (King et al. 1988), which both cause a displacement of the visual field relative to the head, led to a compensatory shift in the auditory map so that the two maps remained in register.

The site of plasticity for this cross-modal calibration of the auditory map in mammals is not known, but there are several indications that this is likely to be within the SC itself. First, the external cortex of the inferior colliculus (ICx) and the nucleus of the brachium of the inferior colliculus (nBIC), the main sources of ascending auditory inputs (Edwards et al. 1979; King et al. 1998a), contain only coarse or partial spatial maps (Binns et al. 1992; Schnupp and King 1997), whereas the dSC is apparently the only midbrain area to contain a complete topographic representation of both sound azimuth and elevation (King and Hutchings 1987; Middlebrooks and Knudsen 1984; Palmer and King 1982). Second, partial aspiration of the sSC in neonatal ferrets impairs the emergence of auditory topography in the region of the dSC underlying the aspirated sSC (King et al. 1998b). This can be explained by loss of the topographically organized input from the sSC to the dSC (Behan and Appell 1992; Doubell et al. 2003), although the presence of a projection from the sSC to the nBIC (Doubell et al. 2000) leaves open the possibility that visual signals could shape auditory responses at an earlier level of the pathway. These results do indicate, however, that the topographic visual signals necessary for refinement of the auditory representation are projected through the sSC.

Address for reprint requests and other correspondence: I. Skaliora, University Laboratory of Physiology, Parks Road, Oxford OX1 3PT, UK (E-mail: irini.skaliora@physiol.ox.ac.uk).

The costs of publication of this article were defrayed in part by the payment of page charges. The article must therefore be hereby marked "*advertisement*" in accordance with 18 U.S.C. Section 1734 solely to indicate this fact.

So far, very little is known about the circuits that support the integration of the two modalities in the SC. Investigating the synaptic connectivity of these converging sensory inputs is a crucial step toward understanding both how sensory signals are transformed to motor commands and how vision calibrates the auditory space map during development. To do this, it is important to be able to study not only the output of multisensory neurons as manifested in their spiking patterns, but also the integration of subthreshold inputs.

In this investigation we have, for the first time, examined converging synaptic inputs in a slice preparation of the midbrain that contains the multisensory layers of the SC as well as the source of both visual (the sSC) and auditory inputs (the nBIC). The purpose of this study was to assess the incidence of convergence onto dSC neurons from these two regions and to evaluate the synaptic integration properties of subthreshold excitatory postsynaptic potentials (EPSPs) in these neurons.

METHODS

In vitro electrophysiology

Coronal slices of the midbrain (500 μm) from 26 Sprague–Dawley rats aged P11 to P17 were prepared as described previously (Doubell et al. 2000, 2003). All procedures involving animals were approved and licensed by the United Kingdom Home Office following local ethical committee review. Briefly, animals were decapitated and the brains quickly removed and submerged in ice-cold artificial cerebrospinal fluid (aCSF) containing (in mM): 124 NaCl, 26 $NaHCO_3$, 2.5 $CaCl_2$, 2.3 KCl, 1.26 $KHPO_4$, 1.0 $MgSO_4$, and 10 D-glucose, bubbled with 95% O_2-5% CO_2. Slices were cut with a Vibraslicer (Campden Instruments, Sileby, UK) and placed in oxygenated aCSF at room temperature. After 30–60 min of incubation, the slices were transferred to the stage of an upright microscope (Axioskop FS, Carl Zeiss, Welwyn Garden City, UK) equipped with video-enhanced DIC optics, and were continuously superfused with aCSF.

Individual cells in the dSC were visualized with Nomarski optics with the use of a ×63 water immersion objective. Suitable cells were identified morphologically in the *stratum griseum intermediale* (layer IV). Typically, recorded cells were large and their somata were round, oval, or pyramidal in shape, having 1 or 2 prominent dendrites. Whole cell patch-clamp recordings were made under visual control with thin glass wall electrodes containing (in mM): 120 potassium gluconate, 10 KCl, 10 EGTA, 10 HEPES, 2 $CaCl_2$, 2 $MgCl_2$, 2 ATP-Na, as well as 0.5% biocytin to stain the recorded neurons. The resistance of the electrodes was 8–11 MΩ in the bath solution. Most recordings were performed at room temperature (23–24°C), although some experiments were done at more physiological temperatures (32–34°C) for comparison. Because no differences were found between the 2 conditions, the data are pooled together. Where appropriate, 4 μM bicuculline or 100 μM picrotoxin were applied to the bathing solution to block inhibitory synaptic activity.

Data acquisition

Electrical stimuli (0.02 ms, 3–100 V; frequency of 0.2–1.0 Hz, or 20 Hz) were applied to *1*) the sSC, through a double-barreled (Θ-shaped) glass pipette filled with extracellular saline (tip diameter: 50–100 μm), and *2*) the nBIC, through a Teflon-coated bipolar silver wire (diameter: 200 μm) (Harvard Apparatus, Holliston, MA). The sSC stimulating electrode was positioned close to the border of the stratum griseum superficiale (layer II) and the stratum opticum (layer III) (Figs. 3, 6, 7), with the aim of stimulating the cell bodies of neurons in these layers while avoiding the spread of depolarization into the dSC (layer IV) itself. For some dSC recordings, a large number of sSC electrode positions were tested, to determine the mediolateral extent of effective stimulation sites. In these cases, we also typically varied the dorsoventral location of the stimulating electrode, but nevertheless stayed close to the layer II–III border. Stimulus strength was increased gradually until an evoked EPSP was visible. Usually, each file included 50 repetitions of the stimulus. After conventional amplification (Axoclamp-2B, Axon Instruments, Foster City, CA), the data were digitized at 20 kHz and fed into a computer (Power Mac, Apple; ITC-16 interface and Axograph software, Axon Instruments).

To examine whether subthreshold responses from the two modalities sum linearly at the soma, stimuli applied at the nBIC and sSC were timed appropriately to ensure the EPSPs evoked in the recorded cell were temporally coincident. In practice, a 5-ms offset between nBIC (first) and sSC (second) stimuli was sufficient for this purpose, given that nBIC latencies were usually between 9 and 12 ms, and sSC latencies between 4 and 7 ms (see RESULTS).

To assess whether subthreshold EPSPs from the two modalities were temporally independent, nBIC and sSC stimuli were separated by 50 ms. The interval of 50 ms was selected to facilitate comparison with other studies (e.g., Clark and Collingridge 1996; Lohmann and Algür 1995; Margulis and Tank 1998) and also because at that interval it was possible to consistently obtain distinct measurable EPSP peaks. Both nBIC followed by sSC, and sSC followed by nBIC stimulations were performed. For comparison, paired-pulse stimulation of the same projections was carried out to assess homosynaptic facilitation or depression: both nBIC and sSC were stimulated twice separately, at an interval of 50 ms. During these protocols, responses to single stimuli were recorded again for comparison.

Data analysis

Onset and peak latencies of the evoked postsynaptic potentials were measured manually for each of the 50 traces in each file and plotted as a function of time. We used the following measures to indicate the latency variability: *1*) the average latency for all of the traces in each file; and *2*) the latency jitter, defined as the range (in ms) between the shortest and longest latency for a given input onto a given cell. We used a combination of both measures to provide evidence for direct connectivity of both EPSPs and IPSPs, as explained in the RESULTS. For cells that displayed putative monosynaptic responses after stimulation of both nBIC and sSC, the amplitude of the initial peak and the integral of the first 20 ms of the EPSP were measured using Axograph software. All measurements were based on the averaged traces of all trials uncontaminated by large voltage fluctuations or spikes. Measurements were taken from the baseline average resting potential in the 1- to 5-ms interval after the stimulus artifact had decayed (and before EPSP onset). For the temporal independence protocols, the first EPSP of the 2 pulses (either hetero- or homosynaptic) was subtracted from the trace to allow calculation of the second EPSP amplitude.

EPSP values are expressed as amplitudes relative to the control, single-stimulation protocol. Data were calculated as percentage values individually for each cell and then averaged over the group. In all cases, paired, 2-tailed *t*-tests were performed on the pairwise raw amplitude data (in mV), because it was the within-cell facilitation or depression of EPSP amplitudes contingent on simultaneous or prior stimulation that was the crucial test of multisensory interaction. Percentage facilitation (or depression) and temporal independence were calculated as follows

LINEAR SUMMATION

$$(EPSP_{nBIC+sSC})/(EPSP_{nBIC} + EPSP_{sSC}) \times 100\%$$

TEMPORAL INDEPENDENCE

$$\text{sSC heterosynaptic stimulation:} \quad (EPSP_{nBIC \Rightarrow sSC})/(EPSP_{sSC}) \times 100\%$$

$$\text{sSC homosynaptic stimulation:} \quad (EPSP_{sSC \Rightarrow sSC})/(EPSP_{sSC}) \times 100\%$$

nBIC heterosynaptic stimulation: $(EPSP_{sSC \Rightarrow nBIC})/(EPSP_{nBIC}) \times 100\%$

nBIC homosynaptic stimulation: $(EPSP_{nBIC \Rightarrow nBIC})/(EPSP_{nBIC}) \times 100\%$

where

$EPSP_{nBIC+sSC}$ = nBIC- and sSC-EPSPs occur simultaneously

$EPSP_{sSC}$ = sSC-EPSP occurs alone

$EPSP_{nBIC \Rightarrow sSC}$ = sSC-EPSP preceded by nBIC-EPSP

$EPSP_{nBIC}$ = nBIC-EPSP occurs alone

$EPSP_{sSC \Rightarrow nBIC}$ = nBIC-EPSP preceded by sSC-EPSP

Histology

To visualize the recorded neurons by biocytin staining, the patch pipettes were carefully detached from the cells and the slices were fixed with 4% paraformaldehyde for several days at 4°C. The slices were subsequently serially sectioned at 50 μm on a sliding microtome (Leica Microsystems, Milton Keynes, UK), incubated with ABC (PK-6100, Vector Labs. Peterborough, UK), washed, and processed with diaminobenzidine (DAB) to obtain a permanent labeling.

In vitro tract tracing experiments

Twenty-one Sprague–Dawley rats, aged P7–P16, were used for neuronal tracer injections in the nBIC. All animals were anesthetized (20% pentobarbitone, intraperitoneally) and perfused transcardially with 10 ml of ice-cold aCSF to wash out most of the blood that could interfere with the later histological procedures. After that, the cortex was removed, and the midbrain blocked between the thalamus and the inferior colliculus before rapid chilling in ice-cold oxygenated aCSF. The midbrain was then either sliced at 500 or 1,000 μm using a Vibraslicer (Leica Microsystems) ($n = 7$ animals) or left intact and just divided along the midline (hemisected brains) ($n = 14$ animals).

Brain preparations were equilibrated at room temperature for at least 10 min before the tracer injection. The tracers used were biotinylated dextrans of 3,000 MW coupled with fluorescein (D-7156, Molecular Probes, Eugene, OR) or tetramethylrhodamine (D-7162, Molecular Probes).

The tracers were injected by iontophoresis using a positive current of 0.5–2.5 mA for 5–10 min with a 50% duty cycle of 7 s. The tracers were allowed to transport for 9–11 h by keeping the tissue in oxygenated aCSF at room temperature. The tissue was fixed by immersion in 4% paraformaldehyde and 1% glutaraldehyde in 0.1 M phosphate buffer (PB) overnight, then embedded in 2% agar and cryoprotected in 30% sucrose PB before serial sectioning at 40 μm on a freezing microtome. The sections were washed in 0.2% Triton X-100 PB, and the endogenous peroxidase was blocked before incubation with ABC for 90 min or overnight. After washing in PB, ABC was reacted with DAB or DAB with nickel to produce a colored precipitate in labeled structures. At least one of the series of sections was counterstained with cresyl violet to enable histological boundaries to be identified.

RESULTS

nBIC projection to the SC

Previous studies in several species (reviewed in King et al. 1998a) have indicated that the dSC receives a substantial auditory projection from the inferior colliculus (IC), the largest component of which comes from the nBIC. An IC-to-dSC projection has also been described in the rat (Cadusseau and Roger 1985; Druga and Syka 1984), but the regions of the IC that supply the SC afferents have not been identified. For this reason we first sought to confirm whether the nBIC-to-dSC pathway is robust in this species.

All the injections made in midbrain slices were confined to the nBIC (Fig. 1, *A* and *B*). Although the tracers used are transported mainly in an anterograde direction, some retrogradely labeled cells were observed, typically in the vicinity of the injection site in the nBIC itself and very occasionally in layer IV of the ipsilateral SC (Fig. 1*D*). In contrast to our previous in vivo retrograde tracing studies in ferrets (Doubell et al. 2000), we did not find any back-filled neurons in the sSC, but this is more likely to reflect the use of slices in the present study than a species difference. In all cases a distinct bundle of labeled fibers emerged from the injection site in the nBIC and ran toward the ipsilateral SC, entering by the most ventral part of the intermediate white matter (layer V) and following a ventrolateral to dorsomedial direction (Fig. 1*B*). Along the fibers' trajectory in layer V numerous clusters of terminals were observed (asterisks in Fig. 1*C*), some of them located in layer V itself, but also in the adjacent layers IV and VI. Several collaterals arose orthogonally from the parent axon in layer V (Fig. 1*C*) to reach more dorsal locations in layer IV where they ramified and gave rise to terminal boutons. In Nissl-stained sections terminal boutons were seen in the proximity of the somata but not apposed to them.

The tracer injections in the hemisected brains were also located in the nBIC. We observed essentially the same projection pattern to the SC as that obtained in slices, although, in the larger hemisected preparation, more axons were labeled and some of these reached the medial aspect of the SC (Fig. 2*A*). The hemisected brain also allowed us to examine the connectivity between the nBIC and other parts of the auditory midbrain. Typically, we observed some labeled neurons in the ICx (Fig. 2*C*) and central nucleus (CNIC) of the inferior colliculus and also in the intercollicular tegmentum (Fig. 2*B*). In addition to these retrogradely labeled cells in the inferior colliculus, some labeled terminals were found in the medial geniculate body (MGB) (Fig. 2*A*). There was a direct relationship between the number of labeled cells in the IC, particularly in the CNIC or rostral pole, and the profusion of terminals in the MGB, especially in its ventral division. It is likely that the MGB labeling resulted from tracer uptake by fibers of passage through the injection site because axons from the IC to the MGB pass through the nBIC.

In summary, these tracer injections show that the rat nBIC is innervated by the auditory midbrain and, in turn, projects to the dSC. The nBIC-dSC axons were found to lie within the coronal plane, revealing that this is an appropriate slice orientation for investigating whether dSC cells respond to stimulation of both the sSC and nBIC.

Synaptic connectivity and convergence

Whole cell recordings were obtained from 70 cells in the dSC and electrical stimulation was applied to the sSC and/or the nBIC (Fig. 3*A*). Electrical stimulation was applied through a theta-glass electrode positioned at different sites across the mediolateral extent of the sSC (Fig. 3*A*), to examine whether the distribution of effective stimulation sites conformed with the columnar organization of the sSC-dSC projection that has been described in different species (Behan and Appell 1992; Doubell et al. 2000, 2003; Lee et al. 1997). If no response was

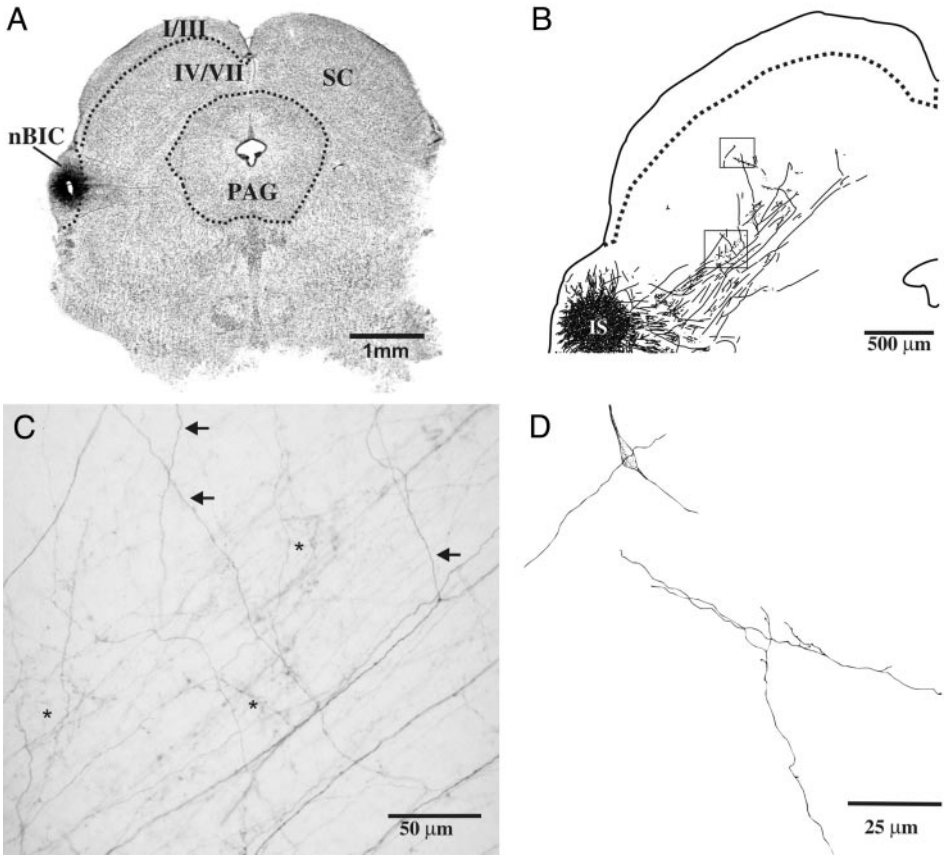

FIG. 1. Projection from the nucleus of the brachium of the inferior colliculus (nBIC) to the superior colliculus (SC) after an injection of Dextran 3000 MW in an in vitro slice preparation. *A*: photograph of a Nissl-stained coronal section at the level of the injection site in the nBIC. *B*: camera lucida drawing of the adjacent section, showing the axonal trajectory and terminals in deep SC. Boxes indicate the location of the details shown in *C* and *D*. *C*: photomicrograph of the trajectory of nBIC axons and terminals in the deep SC. Some axon collaterals (arrows) run perpendicular to the main trajectory of the axons entering the SC. Asterisks indicate terminal button clusters. *D*: camera lucida drawing of a terminal fiber at a more superficial location in layer IV. Abbreviations: I/III, layers I to III of the SC; PAG, peri-aqueductal gray matter.

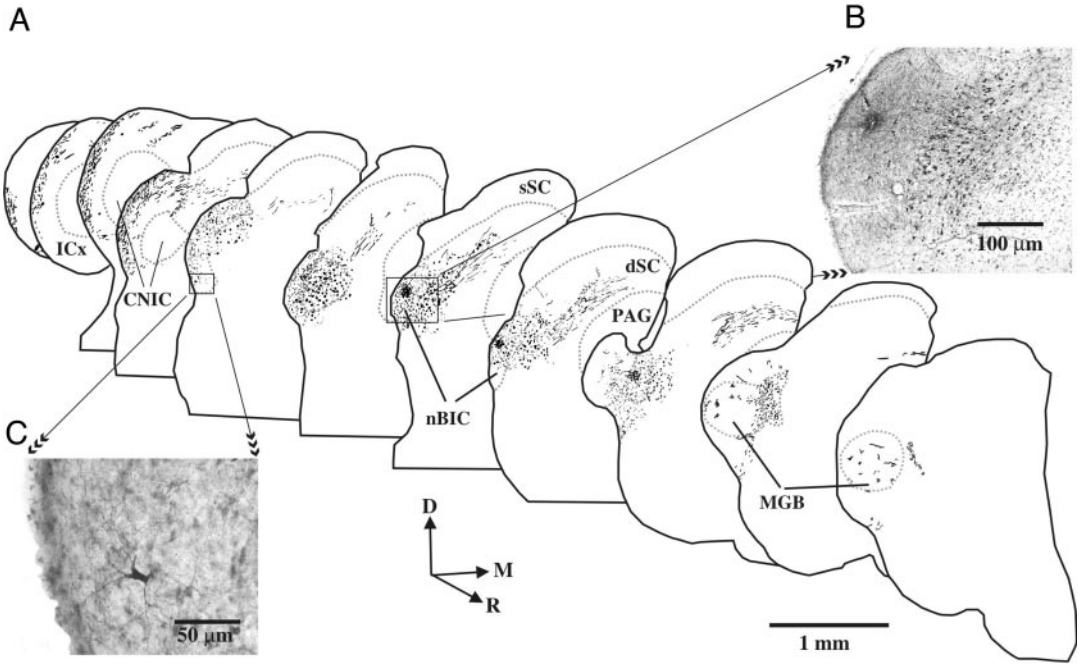

FIG. 2. Projection from the nBIC to the SC in a hemisected midbrain preparation. *A*: camera lucida drawings of the labeled structures seen through serial sections from the inferior colliculus (IC) to the medial geniculate body (MGB). Distance between adjacent sections 200 μm. *B*: photomicrograph showing the injection site in the nBIC and some retrogradely labeled cells medial to it. *C*: retrogradely labeled cell in the external cortex of the IC. Abbreviations: sSC, superficial layers of the superior colliculus; dSC, deeper layers of the superior colliculus; PAG, peri-aqueductal gray matter; nBIC, nucleus of the brachium of the inferior colliculus; ICx, external cortex of the inferior colliculus; CNIC, central nucleus of the inferior colliculus; MGB, medial geniculate body.

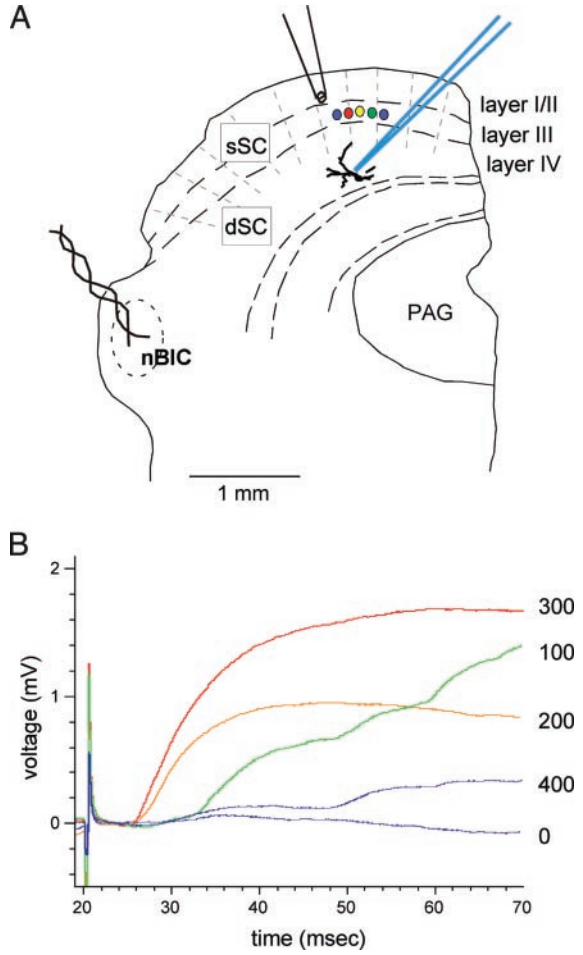

FIG. 3. *A*: schematic diagram of experimental setup. Drawing of coronal slice through the midbrain at the level of the superior colliculus. Stimulation was applied in the sSC and in the nBIC. Whole cell patch-clamp recordings were made from cells in the deeper multisensory layers (dSC). Five colored circles represent 5 consecutive stimulation locations in layer III, which yielded the corresponding responses in *B*. Only one hemisphere is depicted; medial is to the *right* and dorsal to the *top*. *B*: depolarizing intracellular responses of one dSC neuron to electrical stimulation applied at the 5 locations illustrated in *A*. Numbers to the *right* of each trace indicate the relative distance of the stimulation sites in μm, 0 and 400 being the *rightmost* and *leftmost* location, respectively. It can be seen that 100-μm shifts of the stimulating electrode yielded markedly different responses, indicating that a different group of presynaptic cells is stimulated each time. PAG, peri-aqueductal gray.

evoked, the stimulating electrode was moved to one or more different positions. In agreement with out recent finding in ferrets (Doubell et al. 2003), we observed that small shifts of the stimulating electrode by less than 100 μm in the dorsoventral or mediolateral direction could reveal a response where none was there before. This indicates that our method and intensity of stimulation were capable of picking out specific inputs, and that the stimulating current did not spread by more than about 50 μm around the theta electrode. Similarly, such small shifts of the electrode resulted in qualitatively different response patterns (Fig. 3*B*), indicating that distinct groups of cells and axons were being activated at each site.

The data are expressed as the percentage of cells responding relative to the attempts at evoking responses. Of the 56 cells for which electrical stimulation was applied to the sSC, 46 (82%) manifested depolarizing postsynaptic potentials from at least one sSC site. Similarly, of the 45 cells for which electrical stimulation was applied to the nBIC, 24 (53%) manifested depolarizing postsynaptic potentials. Finally, of the 37 cells for which electrical stimulation was applied to both sites, 8 showed no response (22%), whereas 21 cells (57%) gave a response to stimulation of both the sSC and nBIC. These data are summarized in Fig. 4*A*.

Latency analysis

We then examined the latency values and variability of these responses, to estimate the proportion that were likely to be attributable to direct, monosynaptic connections. Response latency for each stimulation site was determined as the average latency of 20–50 sweeps. In those cases where responses were recorded using more than one stimulation site, the site with the shortest latency was included in the average population data.

Latencies of sSC-evoked responses ranged from 4.1 to 12.2 ms (mean ± SD: 6.9 ± 2.1), whereas those from the nBIC were on average about twice as long (range: 6.0–20.3 ms, mean ± SD: 12.8 ± 3.3). However, we found that, in both cases, the *absolute* latency values did not correlate in any simple way with the *latency variability* of evoked responses. Figure 5 shows examples of responses evoked from electrical stimulation in the nBIC in 2 different cells. The first one showed an average response latency of 13 ms and a latency

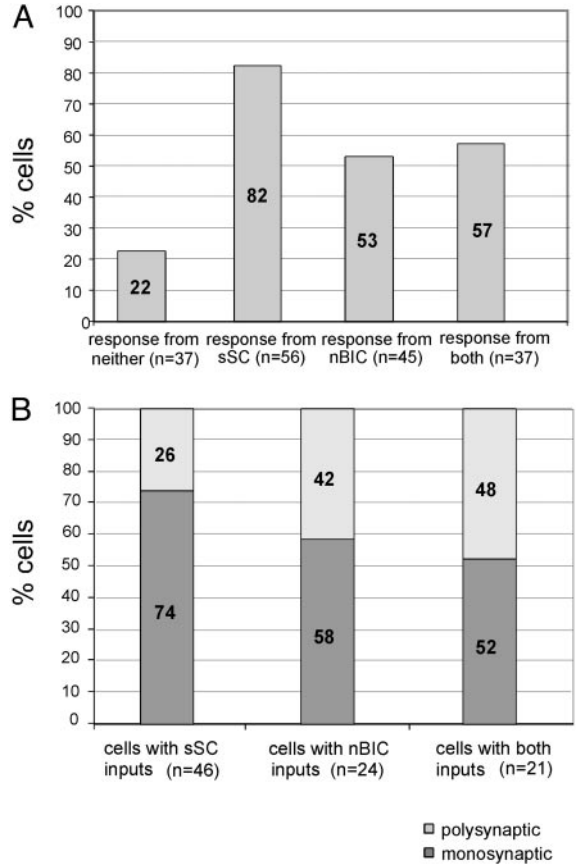

FIG. 4. *A*: summary of the overall functional connectivity from sSC and nBIC to cells in the dSC. Numbers on the bars indicate the percentage of cells responding to neither, sSC, nBIC, or both inputs. *B*: breakdown of the functional connections into monosynaptic and polysynaptic responses. Numbers in parentheses under each bar indicate the number of recorded cells tested in each condition.

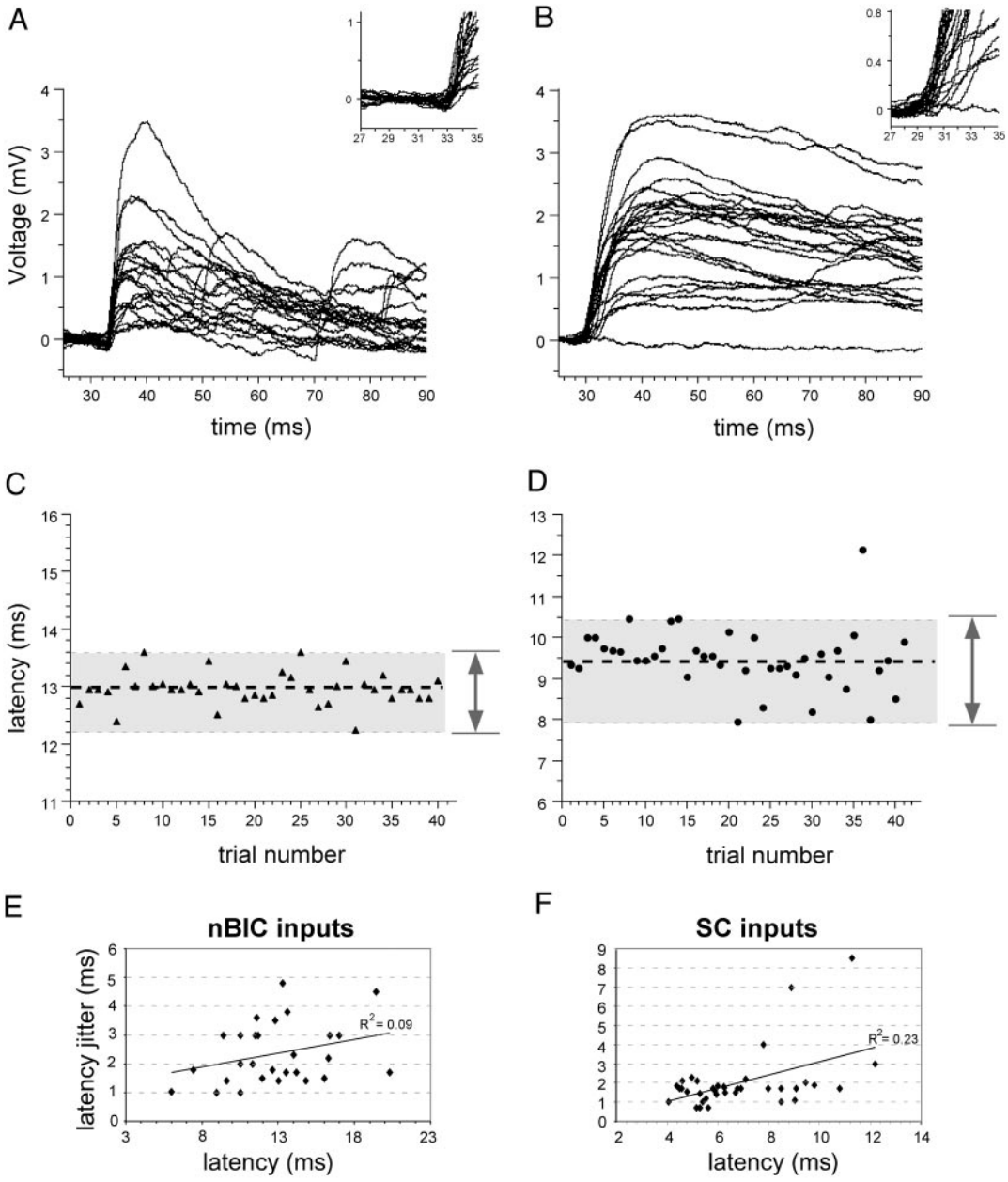

FIG. 5. Examples of evoked responses and latency analysis. *A* and *B*: responses of 2 different cells in the dSC to electrical stimulation in the nBIC. Each trace is a response to a 0.02-ms stimulus applied through a bipolar electrode at 0.2 Hz. *Insets*: illustrate the EPSP onset at higher magnification. *C* and *D*: plots illustrating the latency variability of the evoked responses. Each symbol indicates the latency of one EPSP and latencies are plotted in the order the data were acquired. First cell manifested response latencies ranging from 12.2 to 13.6 ms, whereas the second one had response latencies that ranged from 7.9 to 10.4 ms. Thick dashed lines indicate the mean response latencies in each case (13 and 9.4 ms, respectively). It can be seen that the input to the second cell (*B* and *D*) has a shorter latency than the input to the first cell (*A* and *C*), and yet manifests considerably more variability, even without the one outlier at 12 ms. *E* and *F*: relationship between average latency and latency jitter for the total sample of nBIC and sSC inputs, respectively. Lines represent linear regression fits and the correlation coefficients are indicated next to each line.

jitter of 1.6 ms (Fig. 5, *A* and *C*), whereas the second one had a shorter average latency of 9.4 ms, but a larger jitter of 2.5 ms (Fig. 5, *B* and *D*). Most neurons with short response latencies ($\leq$6 ms) also exhibited low variability ($\leq$2 ms), suggesting the presence of a monosynaptic connection (Fig. 5, *E* and *F*). However, for longer latencies, the correlation was fairly flat, possibly reflecting variability in the degree of myelination of immature fibers. For this reason, a connection was judged to be monosynaptic if either the average latency was $<$6 ms, or the latency jitter was up to 2 ms. The same criteria were applied for all evoked EPSPs, whether they were triggered by stimulation of either the sSC or the nBIC. In the case of the longer latency nBIC-evoked responses, the criterion used was the latency variability, given that the absolute latency of these responses was never below 6 ms. In ambiguous cases, the latency variability to a second pulse applied at 20 Hz was examined. If the variability to the second pulse was similar to that of the first, the response was classified as monosynaptic. However, if

there was a change (±10%) in either failure rate or in the latency jitter, then the response was judged to be polysynaptic.

The results of this analysis are summarized in Fig. 4*B* and indicate that 74% of the 46 dSC cells that received synaptic inputs from the sSC did so through apparently monosynaptic connections (60% of the total population, $n = 56$). The equivalent values for the auditory projection are: 58% of the 24 cells connected to the nBIC received monosynaptic inputs (31% of the total population, $n = 45$). Finally, 52% of cells with convergent inputs ($n = 21$) were adjudged to be monosynaptically connected to both sites. It should be noted that these values represent the lowest estimate of direct connectivity because the likelihood of detecting monosynaptic inputs increased with the number of distinct locations where electrical stimulation was applied.

Functional topography

We examined the degree of functional topography in the projection from the sSC to the dSC. For these experiments we recorded from dSC neurons and stimulated a wide range of sites in the superficial layers, usually covering the entire mediolateral extent of the ipsilateral sSC. The stimulation intensity was kept constant and the electrode was lowered into the tissue to a depth of about 20 μm to keep conditions as similar as possible.

Figure 6 illustrates the responses obtained at different sSC stimulation sites for 4 different dSC neurons. The diagrams on the *left* provide a qualitative illustration of the degree of functional topography present in each case: blue dots represent sites where stimulation was applied but no response was evoked, whereas green and red dots are sites where identical stimulation evoked a polysynaptic or monosynaptic EPSP, respectively. The locations of the recorded neurons are indicated by the black circles in the deep layers. Such maps were obtained from a total of 8 cells in dSC and in 6 cases the topography was similar to the type shown in the first 3 examples (Fig. 6, *A–F*). In the remaining 2 neurons the connectivity was more widespread, as shown in the *bottom panel* (Fig. 6, *G* and *H*). The plots on the *right* of each map illustrate the magnitude of the response evoked from each stimulation site for the corresponding cells. To generate these graphs the integral of the evoked EPSP was calculated for each site, for a 40-ms range after EPSP onset, and the values plotted as a function of horizontal distance within the sSC. Although the largest response was usually generated by putative monosynaptic connections, this was not always the case (e.g., Fig. 6*B*), possibly reflecting differential presynaptic recruitment.

To provide a more quantitative description of the degree of functional topography we measured the extent of monosynaptic and overall (mono- and polysynaptic) connectivity for each of these 8 cells (see Table 1 for individual values). Responses that were adjudged to be monosynaptic were most likely to be elicited by stimulation of layer III and were obtained from a narrower range of stimulation sites than those evoking polysynaptic EPSPs. The average horizontal spread of sSC to dSC connections was 482 ± 497 μm (monosynaptic) and 1148 ± 484 μm (overall).

Taken together, these results indicate that dSC cells receive spatially restricted, apparently monosynaptic inputs from the sSC, as early as the second postnatal week. This precocious topography prompted us to examine whether GABAergic inhibition is sculpting the topographic connectivity from a more widespread excitatory projection. To address this issue we carried out further functional mapping experiments in the presence of the $GABA_A$ receptor blocker picrotoxin (100 μM). Examples of the maps yielded under these conditions are illustrated in Fig. 7. The main difference that is immediately obvious from the maps on the *left* is that there appear to be multiple, discrete sites that are monosynaptically connected to the dSC cells, whereas in control solution that was not the case (compare Figs. 6 and 7). Quantification of the extent of connectivity in all 5 cells for which complete maps were generated revealed that the average horizontal spread for apparently monosynaptic connectivity under $GABA_A$ blockade was nearly 3 times that for the control solution (1395 ± 693 μm), whereas the horizontal spread for overall connectivity was increased by about 50% (1778 ± 327 μm).

Subthreshold linearity

To determine the extent to which EPSPs from the two modalities sum linearly as measured at the soma, we recorded EPSPs from dSC cells while simultaneously stimulating the two inputs. Recordings were performed in the presence of 4 μM bicuculline to block $GABA_A$-mediated IPSPs. Cells were selected that received monosynaptic inputs from both sites and electrical stimulation was applied to the sSC and the nBIC with a temporal offset of 5 ms (to account for the shorter latency of the sSC-evoked response). Following earlier studies of input summation (Burke 1967; Langmoen and Andersen 1983), we refer to the EPSP resulting from simultaneous activation of the two inputs as the "observed sum" and use the term "arithmetic sum" for the computer-added, separately activated inputs (Fig. 8*A*). In most cases combined stimulation resulted in EPSPs that deviated little from the arithmetic sum of the two separately evoked EPSPs, producing a population average of 96.7 ± 3.4% of the arithmetic sum. This small difference was not statistically significant (2-tailed, paired *t*-test, $P = 0.10$). Linearity values for all individual cells ($n = 17$) are shown in Fig. 8*B*. We also examined to what extent deviations from linearity were dependent on the amplitude of the responses (either separate or combined) and/or the natural variability in membrane potential. Neither was found to be a reliable predictor of linearity, as indicated in Fig. 8, *C* and *D*.

Temporal independence

We finally examined whether an EPSP evoked by stimulation of one site could affect a closely following EPSP resulting from stimulation of the other site. To assess this we applied paired-pulse stimulation to the nBIC and sSC sites in cells that received putative monosynaptic inputs from both. The stimuli were temporally offset by 50 ms in either direction, as explained in METHODS. Figure 9 illustrates one such example where sSC-evoked EPSPs (first group of traces) are followed by nBIC-evoked EPSPs (Fig. 9*A*). After the sSC-evoked response was subtracted out, the average of the nBIC-evoked response (Fig. 9*B*, *red trace*) was superimposed on the average nBIC-EPSP evoked on its own (*green trace*). The near-perfect matching of the *red* and *green traces* indicates that a closely preceding sSC-evoked EPSP had no discernable effect on the

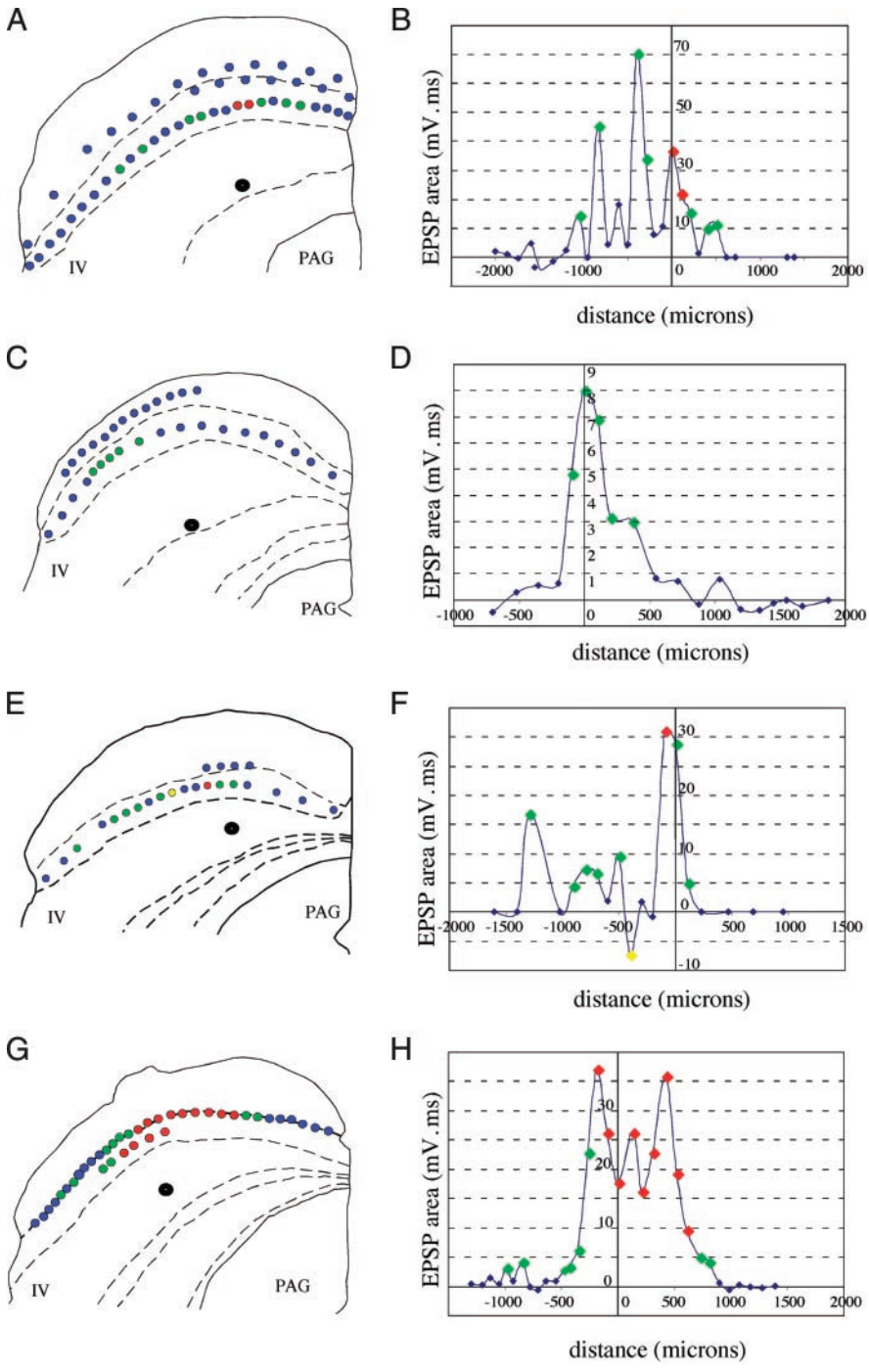

FIG. 6. Functional topography of superficial-to-deep SC projection. *Left panels* (*A, C, E, G*) illustrate the extent of functional connectivity between the layers. Theta-stimulating electrode was moved systematically within the sSC to identify the location of effective stimulation sites for the cells recorded in the dSC (black-filled circles). Blue dots indicate sites in the sSC where stimulation was applied but no response was evoked, whereas green- and red-filled dots indicate locations from where polysynaptic and monosynaptic responses were elicited, respectively. Size of the stimulating electrode and the stimulation intensity were kept constant for all sites. *Right panels* (*B, D, F, H*) show the magnitude of the evoked response as a function of horizontal distance along layer III. Evoked responses were quantified by measuring the area under the excitatory postsynaptic potential (EPSP) trace for a 40-ms window from EPSP onset. Dots are similarly color-coded to reflect the stimulation sites as indicated in the corresponding *left-column panels* for each cell. Yellow dot in the *3rd cell from the top* illustrates a negative-going evoked response, indicating that a net inhibitory postsynaptic potential (IPSP) was evoked at this site. Net IPSPs were uncommon under normal recording conditions.

amplitude of the nBIC-evoked EPSP recorded at the somata of layer IV neurons. For comparison, and to confirm that this same input is capable of short-term plasticity, we applied a homosynaptic paired-pulse stimulation protocol to the nBIC site. In this case the nBIC-evoked EPSP manifested pronounced paired-pulse facilitation, as illustrated in both the raw traces (Fig. 9*C*) and in the superimposed averaged traces (Fig. 9*D*). In keeping with Clark and Collingridge (1996), we refer to this interaction as "homosynaptic" and distinguish it from the "heterosynaptic" interaction between the two pathways. This particular example was typical of the entire population ($n = 10$) as indicated in the column chart (Fig. 9*E*), where the lack of heterosynaptic facilitation in nBIC-evoked EPSPs that were preceded 50 ms earlier by sSC-evoked EPSPs (middle gray bar) is compared to the pronounced homosynaptic facilitation of the nBIC inputs on the same cells (white bar). The difference in EPSP amplitude between a single pulse (1.24 ± 0.16 mV) and the second pulse in a homosynaptic paired-pulse stimulation protocol (2.23 ± 0.32 mV) was significant (2-tailed, paired *t*-test, $P = 0.0004$).

The same qualitative result was found when the temporally opposite effect was examined (i.e., when nBIC-evoked EPSP preceded sSC-evoked EPSP by 50 ms). Again the EPSP evoked by the second pulse in the protocol (sSC) was not significantly different from the EPSP evoked by a single sSC stimulation pulse ($P = 0.87$), whereas the homosynaptic

TABLE 1. *Lateral extent of superficial layer stimulation sites that evoked EPSPs in individual deep layer neurons*

Cell	Age	Polysynaptic Range, μm	Monosynaptic Range, μm	Overall Range, μm
		Control		
SC40	P16	1,400	100	1,400
SC41	P14	470		470
SC42	P12	1,790	710	1,790
SC43	P14	1,550	100	1,550
SC44-1	P11	460		460
SC44-1.2	P11	1,300		1,300
SC44-2.2	P11	100	1,250	1,250
SC45-1	P12	400	250	960
Mean		934	482	1,148
SD		642	497	484
Min		100	100	460
Max		1,790	1,250	1,790
		Plus picrotoxin		
SC46-1.1	P12	910	1,910	1,910
SC46-2.2	P12	2,140	1,790	2,140
SC47-1	P13	1,300	390	1,300
SC48-1	P14	1,610		1,610
SC48-2.1	P14	1,930	1,490	1,930
Mean		1,578	1,395	1,778
SD		491	693	327
Min		910	390	1,300
Max		2,140	1,910	2,140

paired-pulse protocol resulted in a significant facilitation of the second EPSP ($P = 0.036$; Fig. 9*F*).

These results indicate that, although both sensory inputs are capable of undergoing homosynaptic short-term synaptic plasticity, nBIC-evoked EPSPs do not interact with sSC-evoked EPSPs when these are induced in close temporal succession.

DISCUSSION

This study is the first detailed investigation of converging synaptic potentials evoked in deep layer "multisensory" SC neurons by stimulation of the sSC (visual pathway) and the nBIC (auditory pathway). Because this circuit is a likely site for the visually guided development of the auditory space map in the SC, elucidating the properties of synaptic convergence and integration is an important step in understanding both the mechanisms underlying synaptic plasticity as well as the processing of multisensory information.

Multisensory circuits in the slice: specificity of afferent inputs

An important assumption in this study is that we are stimulating independently cells in visual and auditory structures/pathways, that is, that there is no cross talk between the afferent fibers that are activated by the stimulating electrodes placed in the sSC and nBIC. This seems a reasonable assumption for several reasons. It is known that the sSC is an almost exclusively visual area that receives topographically ordered retinal inputs, as well as descending inputs from primary visual cortex (Huerta and Harting 1984). These afferent connections develop early and a mature map of visual space is present at the time of eye opening (Chalupa et al. 1996; Kao et al. 1994; King et al. 1996). Furthermore, we and others have shown that the sSC–dSC pathway is preserved in a coronal slice preparation (Doubell et al. 2003; Isa et al. 1998; Özen et al. 2000; Pettit et al. 1999).

Anatomical studies in several species have shown that the nBIC provides a large projection to the dSC (Edwards et al. 1979; King et al. 1998a) and recordings in both ferrets (Schnupp and King 1997) and cats (Aitkin and Jones 1992) have confirmed that nBIC neurons are acoustically responsive and have spatially tuned receptive fields. The tracing data presented here show that nBIC neurons extend axons that terminate in the dSC, suggesting that this pathway is also likely to provide a major route in by which auditory information reaches the SC in rats. The presence of retrogradely labeled cells in the ICx and CNIC in our hemisected midbrain preparation raises the possibility that some of the labeled axons in the SC were fibers of passage originating from these auditory structures. However, the projection from other regions of the IC to the nBIC (Doubell et al. 2000; Wenstrup et al. 1994) could also account for those retrogradely labeled neurons. Moreover, projections from elsewhere in the IC to the dSC are less likely to be functional in the slices because most of the axons would have been sectioned during the preparation of the slices. Even if a small component of the EPSPs recorded in the SC reflect the activation of axons from regions of the IC other than the nBIC, this does not alter our conclusions on the convergence of visual and auditory inputs in the dSC.

Cross-modal connectivity in the superior colliculus

Recent in vitro studies in different species have documented the existence of functional connections between the superficial visual and deeper multisensory layers of the SC (Doubell et al. 2003; Isa et al. 1998; Lee et al. 1997; Özen et al. 2000). We found that, of the sample of dSC neurons recorded, most (>80%) receive inputs from the sSC and that, in more than half of these, the connection is apparently monosynaptic. In addition, we found that many of the dSC neurons tested received converging inputs from the sSC and nBIC, and, on the basis of the small latency variability, half of those cells apparently received monosynaptic inputs from both regions. Although visual–auditory neurons are widespread in the guinea pig dSC (King and Palmer 1985), electrophysiological recordings in rats (Westby et al. 1990) and other rodents (Chalupa and Rhoades 1977; Dräger and Hubel 1975) have reported a low incidence of multisensory neurons. However, measurements of the expression profiles of the mRNA and protein products of the immediate-early gene *zif268* suggest that most auditory neurons in the dSC of the rat are also visually responsive. This clearly accords with the convergence patterns of synaptic inputs revealed in the present study.

In vivo extracellular recordings in cats have reported that multisensory responses are absent in young animals and emerge gradually, beginning at about 2 wk after eye opening (Wallace and Stein 1997), whereas in monkeys, which are born with their eyes open, multisensory responses are apparent from birth (Wallace and Stein 2001). It is highly likely that the strong projection from the nBIC to the dSC that we observed at least in part underlies the auditory sensitivity of rat SC neurons (Gaese and Johnen 2000). The contribution of sSC

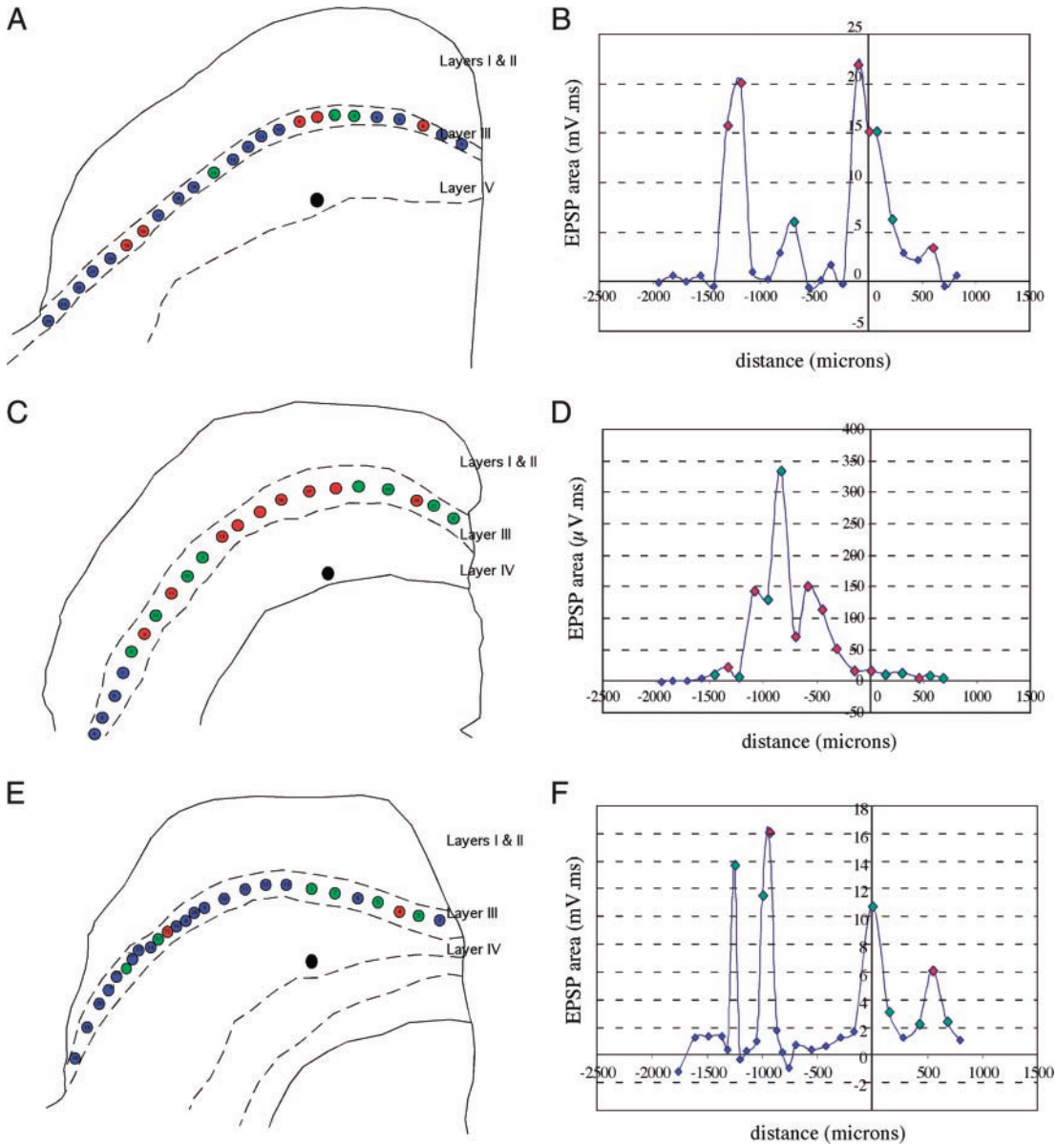

FIG. 7. Effect of $GABA_A$ blockade on the range of effective stimulation sites in the sSC. *Left panels* (*A*, *C*, *E*) and *right panels* (*B*, *D*, *F*) were generated as described for Fig. 6, except that 100 μM picrotoxin was added to the extracellular solution. It can be seen that, in the presence of picrotoxin, dSC cells receive inputs from more widespread regions of the sSC. As before, blue, green, and red dots indicate locations in which stimulation elicited no response, polysynaptic EPSPs and monosynaptic EPSPs, respectively.

inputs to the visual responses of rat dSC neurons is not known, although studies in other rodents have shown that those responses are derived from the sSC (Mooney et al. 1992). Our results therefore suggest that, at around the time of eye opening and the onset of hearing (Friauf 1992), there exists a well-developed circuitry that could support multisensory interactions. Assuming multisensory maturation in rats is similar to that described in a wide range of other species (King 1999), they also show that visual inputs from the sSC are in place to guide the maturation of the auditory spatial responses of dSC neurons.

Superficial deep-layer topography

Our slice recordings suggest that dSC neurons in young rats receive excitatory, monosynaptic inputs from a fairly restricted region of the overlying sSC. Because we were recording from unstained tissue, we were unable to identify unequivocally the precise laminar location of the stimulating electrode. However, our data indicate that the likelihood of evoking monosynaptic responses increased when the electrode was close to the layer II–layer III border or within layer III. This is in agreement with the anatomical studies of sSC-dSC connections in the tree shrew by Hall and Lee (1997). Moreover, a comparable degree of columnar organization—although one that does not differentiate between mono- and polysynaptic connections—has also been reported in SC slices from young (P8–28) tree shrews (Lee et al. 1997).

We found that the topographic order in this pathway is partly shaped by the selective inhibition of a broader set of available connections. Evidence for this comes from a limited sample of

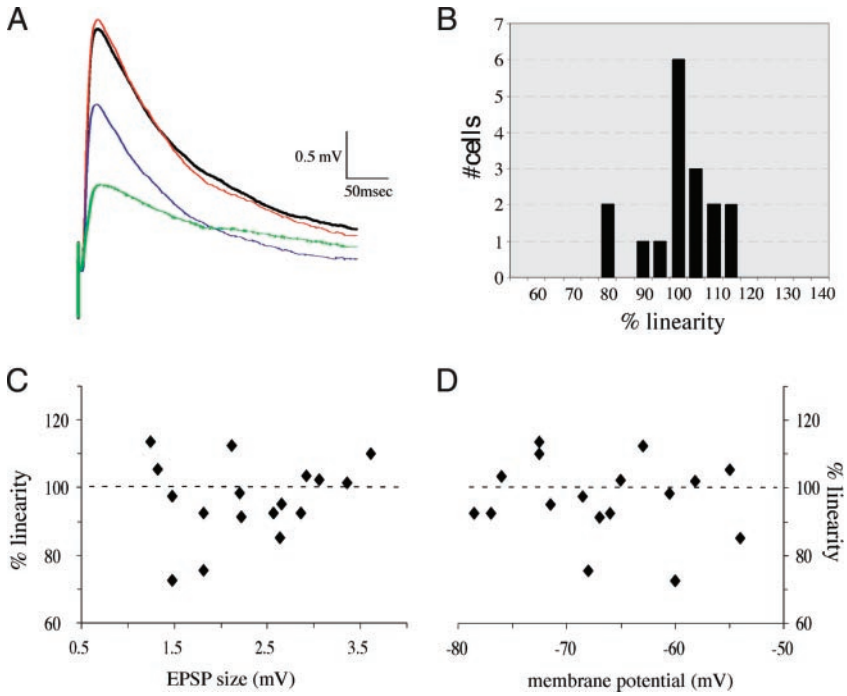

FIG. 8. Linear summation of subthreshold-evoked responses. *A*: responses of a cell to separate stimulation of the nBIC (blue) and sSC (green) are superimposed on the arithmetic sum of the 2 (red) as well as the response to simultaneous stimulation of each site (black). Near-perfect matching of the *red* and *black traces* in this example indicates minimal deviation from linearity. *B*: histogram showing the linearity values for each of the recorded cells ($n = 17$). Linearity did not correlate with either the size of the combined EPSP (*C*) or the membrane potential of the recorded cells (*D*).

neurons, given that exploring the source of inhibition was beyond the scope of the present study. Anatomical data have revealed the presence of numerous GABAergic neurons across all layers of the SC (Appell and Behan 1990; Behan et al. 2002; Mize 1992; Okada 1992; Ottersen and Storm-Mathisen 1984). Also, recordings in both slices and whole animals have revealed an extensive intralaminar network of inhibitory connections by layer IV interneurons (Meredith and Ramoa 1998) or collaterals of layer IV projection neurons (Zhu and Lo 2000). Any of these could have mediated the increase in polysynaptic connectivity we observed, but they cannot explain the unmasking of additional monosynaptic connections from sSC to dSC. Because we did not detect direct monosynaptic inhibitory input from sSC to dSC, the picrotoxin-mediated unmasking of direct sSC–dSC connections could indicate GABA-mediated (selective) failure of spike propagation along the sSC axons (Lamotte et al. 1998; Lomeli et al. 1998; Verdier et al. 2003). Alternatively, or additionally, blocking inhibition globally could increase the number of neurons that are excited within the superficial layers.

Spatial and temporal summation of converging inputs

Recording the response of dSC cells to joint stimulation of sSC and nBIC inputs revealed that the combined response (observed sum) was accurately predicted by the arithmetic sum of the two individual responses. This was true whether the evoked EPSPs were coincident or temporally offset by 50 ms, suggesting that each synaptic input functions independently and that events sum linearly. Linear summation of EPSPs initiated by converging inputs has been reported in other brain areas (Burke 1967; Grabauskas and Bradley 1996; Langmoen and Andersen 1983), although deviations from linearity have been reported as well (Burke 1967; Kogo and Ariel 1999; Nettleton and Spain 2000).

In vivo studies in a range of mammalian species have reported that multisensory inputs can interact to enhance or reduce the spike discharges of dSC neurons (King and Palmer 1985; Meredith and Stein 1983, 1986; Populin and Yin 2002). Estimates of the prevalence and size of these interactions vary, reflecting differences in the species and experimental protocols (e.g., awake vs. anesthetized animals) used and in the definitions used by different authors to define multisensory facilitation. In keeping with other studies of synaptic potentials (e.g., Cash and Yuste 1998; Nettleton and Spain 2000), we defined facilitation as a response to simultaneous activation of the nBIC and dSC that exceeded the sum of the EPSPs to the separately activated inputs.

Although we failed to find evidence for cross-modal interactions in the slice preparation, it is difficult to relate our findings on subthreshold summation of inputs to the response enhancement apparent in the spike output of some dSC neurons in whole animals. A supra-additive (or supralinear) summation of the spike output to combined visual and auditory stimulation may simply reflect a spike threshold condition and need not necessarily rely on a supralinear summation of the underlying synaptic inputs. Linear or even sublinear summation of subthreshold EPSPs can still result in apparent supralinear interactions when assessed by the spike output of cells, if both inputs on their own bring the neuron just below the action potential threshold (Langmoen and Andersen 1983). Alternatively, supralinearity could be a network property (Saito and Isa 2003).

The apparent absence of nonlinear visual–auditory interactions may also reflect the age of the animals, given that in vivo studies in other species have reported that supra-additive responses to bimodal stimulation are first found several weeks after the emergence of sensory responses in the SC (Wallace and Stein 1997, 2001). In cats, the delayed maturation of this integrative property of dSC multisensory neurons appears to be related to the development of corticocollicular inputs (Wallace and Stein 2000). Such inputs are obviously missing in slices prepared from infant animals, which may therefore underesti-

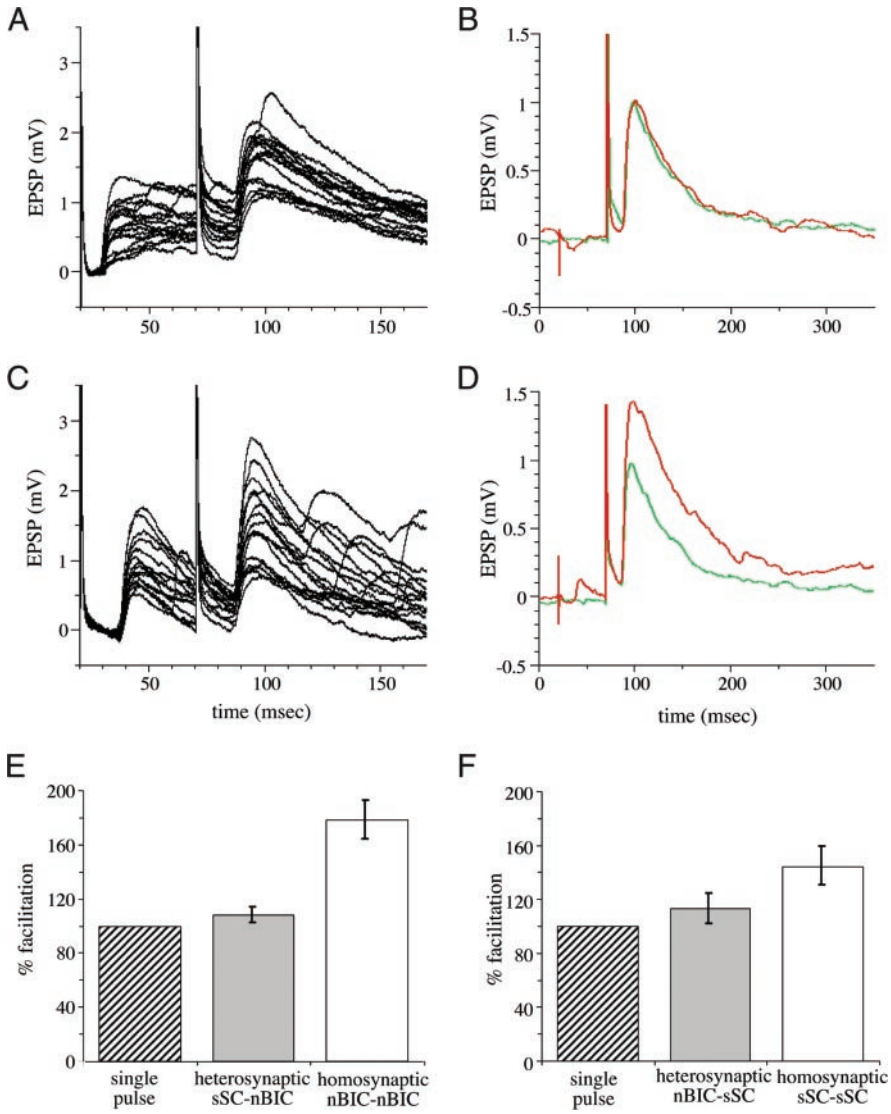

FIG. 9. Temporal independence of nBIC- and sSC-evoked EPSPs. *A*: heterosynaptic paired-pulse stimulation protocol, where electrical stimulation of the sSC is followed by electrical stimulation of the nBIC 50 ms later. First and second group of traces are sSC- and nBIC-evoked responses, respectively. *B*: average EPSPs evoked by separate single stimulation in the nBIC (*green trace*) and by stimulation of the nBIC after stimulation of the sSC (*red trace*). *C*: homosynaptic paired-pulse stimulation protocol, where 2 identical electrical pulses are applied to the nBIC at a 50-ms interval. *D*: average EPSPs evoked by separate single stimulation in the nBIC (*green trace*) and by paired-pulse stimulation in the nBIC (*red trace* illustrates the *second* EPSP in the pair). *E*: percentage facilitation of EPSPs evoked by single nBIC stimulation (single pulse), nBIC stimulation preceded by sSC stimulation (heterosynaptic), and nBIC stimulation preceded by nBIC stimulation (homosynaptic). Whereas the homosynaptic stimulation paradigm revealed significant paired-pulse facilitation, an sSC-induced EPSP evoked at the same interval had no effect on a subsequent nBIC-evoked EPSP. *F*: same result was obtained when the reverse order of stimulation was applied, where an sSC-induced EPSP was preceded by either an nBIC-induced (heterosynaptic) or an sSC-induced response (homosynaptic), respectively.

mate the degree of nonlinearity. Nevertheless, it is likely that future advances in our understanding of the capacity of neurons to synthesize multisensory signals will benefit from both in vivo and in vitro studies of synaptic integration.

Independence of visual and auditory inputs

Paired-pulse stimulation of either input alone revealed a significant degree of homosynaptic paired-pulse facilitation for both sSC and nBIC-mediated EPSPs. In contrast, stimulation of one set of fibers before stimulation of the other set of fibers did not result in any heterosynaptic interactions. This indicates that the depolarization induced by synaptic activation of either the visual or the auditory input does not affect the synapses at the site of the other input. Thus at least at this developmental stage, spread of depolarization from one input to the other, as shown in the hippocampus (Clark and Collingridge 1996), does not appear to underlie any interactions that may take place between the two modalities.

Taken together with the linear summation results discussed previously, our data suggest that, at least at around the time of opening of eyes and ear canals, visual and auditory inputs appear to function independently of each other. Any interactions between them are therefore likely to be mediated by the overall level of activity of the postsynaptic cell.

ACKNOWLEDGMENTS

We are grateful to A. Alli for assistance with the functional topography experiments.

GRANTS

We thank the Wellcome Trust for financial support. A. J. King is a Wellcome Senior Research Fellow.

REFERENCES

Aitkin L and Jones R. Azimuthal processing in the posterior auditory thalamus of cats. *Neurosci Lett* 142: 81–84, 1992.

Appell PP and Behan M. Sources of subcortical GABAergic projections to the superior colliculus in the cat. *J Comp Neurol* 302: 143–158, 1990.

Behan M and Appell PP. Intrinsic circuitry in the cat superior colliculus: projections from the superficial layers. *J Comp Neurol* 315: 230–243, 1992.

Behan M, Steinhacker K, Jeffrey BS, and Meredith MA. Chemoarchitecture of GABAergic neurons in the ferret superior colliculus. *J Comp Neurol* 452: 334–359, 2002.

Binns KE, Grant S, Withington DJ, and Keating MJ. A topographic representation of auditory space in the external nucleus of the inferior colliculus of the guinea-pig. *Brain Res* 589: 231–242, 1992.

Burke RE. Composite nature of the monosynaptic excitatory postsynaptic potential. *J Neurophysiol* 30: 1114–1137, 1967.

Burnett LR, Stein BE, Chaponis D, and Wallace MT. Superior colliculus lesions preferentially disrupt multisensory orientation. *Neuroscience* 124: 535–547, 2004.

Cadusseau J and Roger M. Afferent projections to the superior colliculus in the rat, with special attention to the deep layers. *J Hirnforsch* 26: 667–681, 1985.

Cash S and Yuste R. Input summation by cultured pyramidal neurons is linear and position-independent. *J Neurosci* 18: 10–15, 1998.

Chalupa LM and Rhoades RW. Responses of visual, somatosensory, and auditory neurones in the golden hamster's superior colliculus. *J Physiol* 270: 595–626, 1977.

Chalupa LM, Snider CJ, and Kirby MA. Topographic organization in the retinocollicular pathway of the fetal cat demonstrated by retrograde labeling of ganglion cells. *J Comp Neurol* 368: 295–303, 1996.

Clark KA and Collingridge GL. Evidence that heterosynaptic depolarization underlies associativity of long-term potentiation in rat hippocampus. *J Physiol* 490: 455–462, 1996.

Doubell TP, Baron J, Skaliora I, and King AJ. Topographical projection from the superior colliculus to the nucleus of the brachium of the inferior colliculus in the ferret: convergence of visual and auditory information. *Eur J Neurosci* 12: 4290–4308, 2000.

Doubell TP, Skaliora I, Baron J, and King AJ. Functional connectivity between the superficial and deeper layers of the superior colliculus: an anatomical substrate for sensorimotor integration. *J Neurosci* 23: 6596–6607, 2003.

Dräger UC and Hubel DH. Responses to visual stimulation and relationship between visual, auditory, and somatosensory inputs in mouse superior colliculus. *J Neurophysiol* 38: 690–713, 1975.

Druga R and Syka J. Projections from auditory structures to the superior colliculus in the rat. *Neurosci Lett* 45: 247–252, 1984.

Edwards SB, Ginsburgh CL, Henkel CK, and Stein BE. Sources of subcortical projections to the superior colliculus in the cat. *J Comp Neurol* 184: 309–329, 1979.

Friauf E. Tonotopic order in the adult and developing auditory system of the rat as shown by c-fos immunocytochemistry. *Eur J Neurosci* 4: 798–812, 1992.

Gaese BH and Johnen A. Coding for auditory space in the superior colliculus of the rat. *Eur J Neurosci* 12: 1739–1752, 2000.

Grabauskas G and Bradley RM. Synaptic interactions due to convergent input from gustatory afferent fibers in the rostral nucleus of the solitary tract. *J Neurophysiol* 76: 2919–2927, 1996.

Hall WC and Lee PH. Interlaminar connections of the superior colliculus in the tree shrew. III: The optic layer. *Vis Neurosci* 14: 647–661, 1997.

Huerta MF and Harting JK. The mammalian superior colliculus: studies of its morphology and connections. In: *Comparative Neurology of the Optic Tectum*, edited by Vaneges H. New York: Plenum Press, 1984, p. 687–773.

Isa T, Endo T, and Saito Y. The visuo-motor pathway in the local circuit of the rat superior colliculus. *J Neurosci* 18: 8496–8504, 1998.

Kao CQ, McHaffie JG, Meredith MA, and Stein BE. Functional development of a central visual map in cat. *J Neurophysiol* 72: 266–272, 1994.

King AJ. Sensory experience and the formation of a computational map of auditory space in the brain. *Bioessays* 21: 900–911, 1999.

King AJ and Carlile S. Changes induced in the representation of auditory space in the superior colliculus by rearing ferrets with binocular eyelid suture. *Exp Brain Res* 94: 444–455, 1993.

King AJ and Hutchings ME. Spatial response properties of acoustically responsive neurons in the superior colliculus of the ferret: a map of auditory space. *J Neurophysiol* 57: 596–624, 1987.

King AJ, Hutchings ME, Moore DR, and Blakemore C. Developmental plasticity in the visual and auditory representations in the mammalian superior colliculus. *Nature* 332: 73–76, 1988.

King AJ, Jiang ZD, and Moore DR. Auditory brainstem projections to the ferret superior colliculus: anatomical contribution to the neural coding of sound azimuth. *J Comp Neurol* 390: 342–365, 1998a.

King AJ and Palmer AR. Cells responsive to free-field auditory stimuli in guinea-pig superior colliculus: distribution and response properties. *J Physiol* 342: 361–381, 1983.

King AJ and Palmer AR. Integration of visual and auditory information in bimodal neurones in the guinea-pig superior colliculus. *Exp Brain Res* 60: 492–500, 1985.

King AJ, Schnupp JW, Carlile S, Smith AL, and Thompson ID. The development of topographically-aligned maps of visual and auditory space in the superior colliculus. *Prog Brain Res* 112: 335–350, 1996.

King AJ, Schnupp JW, and Thompson ID. Signals from the superficial layers of the superior colliculus enable the development of the auditory space map in the deeper layers. *J Neurosci* 18: 9394–9408, 1998b.

Knudsen EI and Brainard MS. Visual instruction of the neural map of auditory space in the developing optic tectum. *Science* 253: 85–87, 1991.

Knudsen EI, Esterly SD, and du-Lac S. Stretched and upside-down maps of auditory space in the optic tectum of blind-reared owls; acoustic basis and behavioral correlates. *J Neurosci* 11: 1727–1747, 1991.

Kogo N and Ariel M. Response attenuation during coincident afferent excitatory inputs. *J Neurophysiol* 81: 2945–2955, 1999.

Kudo M and Niimi K. Ascending projections of the inferior colliculus in the cat: an autoradiographic study. *J Comp Neurol* 191: 545–556, 1980.

Lamotte dIB, Destombes J, Thiesson D, Hellio R, Lasserre X, Kouchtir DN, Jami L, and Zytnicki D. Indications for GABA-immunoreactive axo-axonic contacts on the intraspinal arborization of a Ib fiber in cat: a confocal microscope study. *J Neurosci* 18: 10030–10036, 1998.

Langmoen IA and Andersen P. Summation of excitatory postsynaptic potentials in hippocampal pyramidal cells. *J Neurophysiol* 50: 1320–1329, 1983.

Lee PH, Helms MC, Augustine GJ, and Hall WC. Role of intrinsic synaptic circuitry in collicular sensorimotor integration. *Proc Natl Acad Sci USA* 94: 13299–13304, 1997.

Lohmann H and Algur Y. Spatio-temporal summation of synaptic activity in visual cortical pyramidal cells in vitro. *Brain Res* 671: 275–281, 1995.

Lomeli J, Quevedo J, Linares P, and Rudomin P. Local control of information flow in segmental and ascending collaterals of single afferents. *Nature* 395: 600–604, 1998.

Margulis M and Tang CM. Temporal integration can readily switch between sublinear and supralinear summation. *J Neurophysiol* 79: 2809–2813, 1998.

Meredith MA and Ramoa AS. Intrinsic circuitry of the superior colliculus: pharmacophysiological identification of horizontally oriented inhibitory interneurons. *J Neurophysiol* 79: 1597–1602, 1998.

Meredith MA and Stein BE. Interactions among converging sensory inputs in the superior colliculus. *Science* 221: 389–391, 1983.

Meredith MA and Stein BE. Visual, auditory, and somatosensory convergence on cells in superior colliculus results in multisensory integration. *J Neurophysiol* 56: 640–662, 1986.

Middlebrooks JC and Knudsen EI. A neural code for auditory space in the cat's superior colliculus. *J Neurosci* 4: 2621–2634, 1984.

Mize RR. The organization of GABAergic neurons in the mammalian superior colliculus. *Prog Brain Res* 90: 219–248, 1992.

Mooney RD, Nikoletseas MM, King TD, Savage SV, Weaver MT, and Rhoades RW. Structural and functional consequences of neonatal deafferentation in the superficial layers of the hamster's superior colliculus. *J Comp Neurol* 315: 398–412, 1992.

Nettleton JS and Spain WJ. Linear to supralinear summation of AMPA-mediated EPSPs in neocortical pyramidal neurons. *J Neurophysiol* 83: 3310–3322, 2000.

Okada Y. The distribution and function of gamma-aminobutyric acid (GABA) in the superior colliculus. *Prog Brain Res* 90: 249–262, 1992.

Ottersen OP and Storm-Mathisen J. Glutamate- and GABA-containing neurons in the mouse and rat brain, as demonstrated with a new immunocytochemical technique. *J Comp Neurol* 229: 374–392, 1984.

Özen G, Augustine GJ, and Hall WC. Contribution of superficial layer neurons to premotor bursts in the superior colliculus. *J Neurophysiol* 84: 460–471, 2000.

Palmer AR and King AJ. The representation of auditory space in the mammalian superior colliculus. *Nature* 299: 248–249, 1982.

Pettit DL, Helms MC, Lee P, Augustine GJ, and Hall WC. Local excitatory circuits in the intermediate gray layer of the superior colliculus. *J Neurophysiol* 81: 1424–1427, 1999.

Populin LC and Yin TC. Bimodal interactions in the superior colliculus of the behaving cat. *J Neurosci* 22: 2826–2834, 2002.

Saito Y and Isa T. Local excitatory network and NMDA receptor activation generate a synchronous and bursting command from the superior colliculus. *J Neurosci* 23: 5854–5864, 2003.

Schnupp J and King A. Coding for auditory space in the nucleus of the brachium of the inferior colliculus in the ferret. *J Neurophysiol* 78: 2717–2731, 1997.

Stein BE, Magalhaes-Castro B, and Kruger L. Superior colliculus: visuotopic–somatotopic overlap. *Science* 189: 224–226, 1975.

Stein BE and Meredith MA. Multisensory integration. Neural and behavioral solutions for dealing with stimuli from different sensory modalities. *Ann NY Acad Sci* 608: 51–65, 1990.

Stein BE and Meredith MA. *The Merging of the Senses.* Cambridge, MA: MIT Press, 1993.

Verdier D, Lund JP, and Kolta A. GABAergic control of action potential propagation along axonal branches of mammalian sensory neurons. *J Neurosci* 23: 2002–2007, 2003.

Wallace MT and Stein BE. Development of multisensory neurons and multisensory integration in cat superior colliculus. *J Neurosci* 17: 2429–2444, 1997.

Wallace MT and Stein BE. Onset of cross-modal synthesis in the neonatal superior colliculus is gated by the development of cortical influences. *J Neurophysiol* 83: 3578–3582, 2000.

Wallace MT and Stein BE. Sensory and multisensory responses in the newborn monkey superior colliculus. *J Neurosci* 21: 8886–8894, 2001.

Wenstrup JJ, Larue DT, and Winer JA. Projections of physiologically defined subdivisions of the inferior colliculus in the mustached bat: targets in the medial geniculate body and extrathalamic nuclei. *J Comp Neurol* 346: 207–236, 1994.

Westby GW, Keay KA, Redgrave P, Dean P, and Bannister M. Output pathways from the rat superior colliculus mediating approach and avoidance have different sensory properties. *Exp Brain Res* 81: 626–638, 1990.

Withington DJ, Binns KE, Ingham NJ, and Thornton SK. Plasticity in the superior collicular auditory space map of adult guinea-pigs. *Exp Physiol* 79: 319–325, 1994.

Zangenehpour S and Chaudhuri A. Neural activity profiles of the neocortex and superior colliculus after bimodal sensory stimulation. *Cereb Cortex* 11: 924–935, 2001.

Zhu JJ and Lo FS. Recurrent inhibitory circuitry in the deep layers of the rabbit superior colliculus. *J Physiol* 3: 731–740, 2000.